Spin Density Matrix Elements in Exclusive Muoproduction of ρ^0 and ω Mesons at COMPASS

Kamil Augsten[1] on behalf of the COMPASS collaboration

[1]*Czech Technical University in Prague, Prague, Czech Republic*

E-mail: kamil.augsten@fjfi.cvut.cz

Spin Density Matrix Elements (SDMEs) describe the transition processes between initial spin states of the virtual photon and final spin states of the produced vector meson and provide an important input for modelling Generalised Parton Distributions (GPDs). The SDMEs are measured in hard exclusive muoproduction of ρ^0 and ω mesons on the proton using $\pm 80\%$ polarised μ^+ and μ^- beams with energy 160 GeV scattering off a liquid hydrogen target. Significant deviation from the hypothesis of s-channel helicity conservation is observed. The results for exclusive ρ^0 meson show dominant contribution of natural-parity-exchange amplitudes and a small contribution of unnatural-parity-exchange amplitudes at small values of W. On the contrary, results for exclusive ω meson indicate significant contribution of unnatural-parity-exchange amplitudes that decreases with increasing W.

KEYWORDS: Vector mesons, Spin Density Matrix Elements, Generalised Parton Distributions

1. Introduction

Exclusive vector meson production in lepton-nucleon scattering provides a convenient tool for studying the production mechanism and, in a model-dependent way, the structure of the nucleon. Here, we report on exclusive ρ^0 and ω mesons muoproduction:

$$\mu + p \rightarrow \mu' + p' + \rho^0/\omega, \tag{1}$$

which can be approximated by the one-photon-exchange as the interaction of a virtual photon γ^* with the target proton p, process known at high virtuality Q^2 of the photon as Hard Exclusive Meson Production (HEMP).

This process has been traditionally explained by Vector Meson Dominance model using Regge phenomenology to describe virtual photon fluctuation into $q\bar{q}$-pair, which scatters off the nucleon and then hadronize into the final vector meson [1]. A complementary approach of description is provided in the context of perturbative QCD (pQCD), where exclusive meson production at sufficiently large Q^2 and W is assumed to be described by handbag-diagrams that involve various non-perturbative nucleon structure functions linked to Generalized Parton Distributions (GPDs) [2–5].

The spin density matrix elements (SDMEs), observables used to describe how the spin components of the virtual photon are transferred to those of the created vector meson, provide wealth of information on the parton structure of the nucleon and can can provide constraints on GPDs parameterisations beyond those from measurements of cross sections and spin asymmetries for HEMP [6,7].

In leptoproduction as shown in Eq. (1), the spin transfer from the virtual photon to the vector meson is commonly described by helicity amplitudes, from which SDMEs can be constructed. For an unpolarised nucleon target, after summing over initial and final spin states of the proton, SDMEs only depend on the helicities of virtual photon and produced meson. The measured SDME values can be used to establish a hierarchy of helicity amplitudes, to test the hypothesis of s-channel helicity

conservation (SCHC), to evaluate the contribution of unnatural-parity-exchange (UPE) and natural-parity-exchange (NPE) transitions and to assess the role of chiral-odd, i.e. parton helicity-flip GPDs in exclusive vector meson production. They also allow to determine the phase difference between helicity amplitudes as well as the longitudinal-to-transverse cross-section ratio.

2. Experimental setup and data selection

Following measurements are based on 2012 (4 weeks long pilot run) data collected COMPASS experiment, described in Ref [8,9]. CERN SPS North Area μ^+ and μ^- beams with energy of 160 GeV and polarization of $\approx \pm 80\%$ were used (data were taken and recorded separately) on a a 2.5 m long liquid-hydrogen target surrounded by a time-of-flight (TOF) system for the detection of recoiling protons (that is not used for the determination of SDMEs, only for systematic uncertainty checks).

The selected events are required to have a topology as that of the observed process in Eq. (1), where $\rho^0 \to \pi^+ \pi^-$ (BR $\approx 99\%$) and $\omega \to \pi^+ \pi^- \pi^0$ (BR $\approx 89\%$) with additional decay of $\pi^0 \to \gamma\gamma$ (BR $\approx 99\%$). Events should have one reconstructed vertex inside the liquid-hydrogen target associated with the incoming and the outgoing muon (of the same charge), and two hadron tracks of opposite charge. ω decay additionally requires two neutral clusters in the calorimeters. Additional quality criteria on tracks are applied.

The following common kinematic selections are applied to select exclusively produced ρ^0 and ω mesons: $1 < Q^2 < 10$ (GeV/c)^2 (virtuality of exchanged photon), $0.1 < y < 0.9$, $W > 5$ GeV/c^2 (mass of final hadronic system), $0.01 < p_{\mathrm{T}}^2 < 0.5$ (GeV/c)^2 (transverse momentum of the vector meson with respect to the virtual-photon direction). To select ρ^0 mesons: $0.5 < M_{\pi^+\pi^-} < 1.1$ GeV/c^2. To select ω mesons: $0.71 < M_{\pi^+\pi^-\pi^0} < 0.86$ GeV/c^2 and $0.1 < M_{\gamma\gamma} < 0.17$ GeV/c^2. To ensure the exclusivity of the produced mesons, the missing energy

$$E_{\mathrm{miss}} = \frac{M_{\mathrm{X}}^2 - M^2}{2M},\tag{2}$$

where M is the proton mass and M_{X}^2 is the missing mass squared, is constrained by $|E_{\mathrm{miss}}| < 2.5$ GeV for ρ^0 and by $|E_{\mathrm{miss}}| < 3$ GeV for ω meson. Additionally, the E_{miss} distribution is used to determine the fraction of SIDIS background under the exclusive peak with normalization from region 7 GeV $< E_{\mathrm{miss}} < 20$ GeV, following the procedure described in [10].

Applying all selection criteria yields to 52257 events for ρ^0 and 3060 events for ω meson channel.

3. Theoretical formalism and experimental access

The theoretical formalism of SDMEs and helicity amplitudes introduced by K. Schilling and G. Wolf [6] is used. The helicity amplitudes $F_{\lambda_V \lambda_N' \lambda_\gamma \lambda_N}$ describe the transition of a virtual photon with helicity λ_γ to a vector meson with helicity λ_V, where λ_N (λ_N') is the nucleon helicity in the initial (final) state. In the centre-of-mass (CM) system of virtual photon and nucleon, the vector-meson spin density matrix $\rho_{\lambda_V \lambda_V'}$ is related to the helicity amplitude $F_{\lambda_V \lambda_V' \lambda_\gamma \lambda_N}$ as [6]

$$\rho_{\lambda_V \lambda_V'} = \frac{1}{2\mathcal{N}} \sum_{\lambda_\gamma \lambda_\gamma' \lambda_N \lambda_N'} F_{\lambda_V \lambda_N' \lambda_\gamma \lambda_N} \, \varrho_{\lambda_\gamma \lambda_\gamma'}^{U+L} \, F_{\lambda_V' \lambda_N' \lambda_\gamma' \lambda_N}^*,\tag{3}$$

where $\mathcal{N}$ is a normalisation factor. The virtual-photon spin density matrix $\varrho_{\lambda_\gamma \lambda_\gamma'}^{U+L}$ describes the subprocess $\mu \to \mu' + \gamma^*$ and decomposes as [11]

$$\varrho_{\lambda_\gamma \lambda_\gamma'}^{U+L} = \varrho_{\lambda_\gamma \lambda_\gamma'}^{U} + P_b \, \varrho_{\lambda_\gamma \lambda_\gamma'}^{L},\tag{4}$$

where the matrix with superscript L (U) contains elements that are coupled (not coupled) to the beam polarisation P_b, referred as "polarised" ("unpolarised").

After the decomposition of $\varrho^{U+L}_{\lambda_\gamma \lambda'_\gamma}$ into the set of 3×3 Hermitian matrices [6], the vector-meson spin density matrix can be expressed in terms of a set of nine matrices $\rho^\alpha_{\lambda_V \lambda'_V}$ corresponding to different virtual-photon polarisation states. SDMEs are usually defined as follows:

$$r^{04}_{\lambda_V \lambda'_V} = (\rho^0_{\lambda_V \lambda'_V} + \epsilon R \rho^4_{\lambda_V \lambda'_V})(1 + \epsilon R)^{-1},$$

$$r^\alpha_{\lambda_V \lambda'_V} = \begin{cases} \rho^\alpha_{\lambda_V \lambda'_V}(1 + \epsilon R)^{-1}, & \alpha = 1, 2, 3, \\ \sqrt{R}\rho^\alpha_{\lambda_V \lambda'_V}(1 + \epsilon R)^{-1}, & \alpha = 5, 6, 7, 8 \end{cases} \tag{5}$$

as it is not possible to separate the contributions from longitudinally and transversely polarised photons. $R = d\sigma_L/d\sigma_T$ denotes the differential longitudinal-to-transverse cross-section ratio of virtual photons and ϵ is the virtual-photon polarisation parameter. The relations between the 23 SDMEs defined in 5 and the helicity amplitudes are given in [11].

3.1 Experimental access to spin density matrix elements and extraction

SDMEs are extracted from experimental data as fitted parameters of the three-dimensional angular distribution $\mathcal{W}^{U+L}(\Phi, \phi, \cos\Theta)$ to the corresponding experimental distribution. Angles and reference frames are defined in Fig. 1.
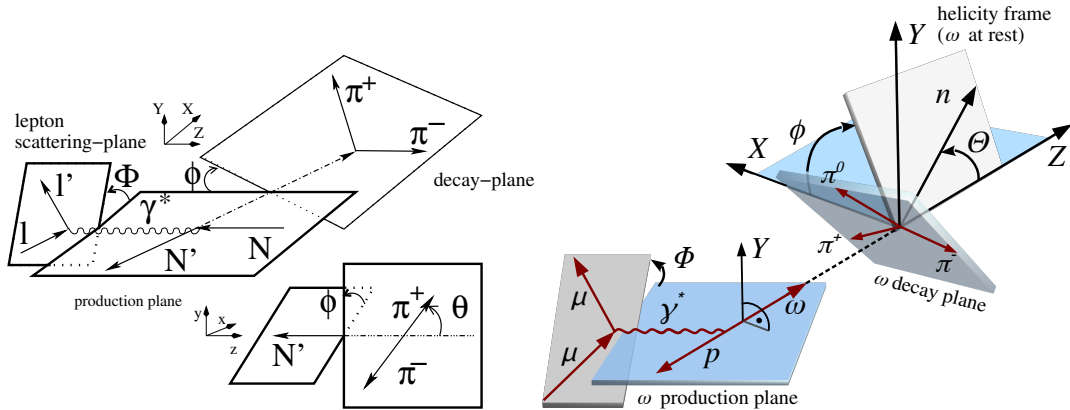

Fig. 1. Definition of angles in the process $\mu N \to \mu N \rho^0(\omega)$ left (right) with $\rho^0 \to \pi^+\pi^-$ (left) and $\omega \to \pi^+\pi^-\pi^0$ (right). Here, Φ is the angle between the meson production plane and the lepton scattering plane in the centre-of-mass system of the virtual photon and the target nucleon, while ϕ is the azimuthal angle that describe the two-pion or three-pion decay of the meson. The variable Θ is the polar angle of decay π^+ in the meson rest frame.

The angular distribution $\mathcal{W}^{U+L}$ is decomposed into contributions that are not coupled ($\mathcal{W}^U$) or coupled ($\mathcal{W}^L$) to the beam polarisation:

$$\mathcal{W}^{U+L}(\Phi, \phi, \cos\Theta) = \mathcal{W}^U(\Phi, \phi, \cos\Theta) + P_b \mathcal{W}^L(\Phi, \phi, \cos\Theta). \tag{6}$$

Using the data, which were collected with a longitudinally polarised beam, 15 "unpolarised" SDMEs are extracted from $\mathcal{W}^U$ and and 8 "polarised" SDMEs from $\mathcal{W}^L$ as described in [12].

Experimentally, the SDMEs are determined by an Unbinned Maximum Likelihood fit of the function $\mathcal{W}(\mathcal{R}; \Phi, \phi, \cos\Theta)$ to the experimental three-dimensional angular distribution of meson production and decay. $\mathcal{R}$ denotes the set of 23 SDMEs $r^\alpha_{\lambda_V \lambda'_V}$. In order to determine SDMEs that are

corrected for SIDIS background, a two-step procedure is used to parameterize background angular distributions and to provide background-corrected SDMEs.

3.2 Systematic uncertainties

The following five sources of systematic uncertainties are considered. First, the difference between results for μ^+ and μ^- beams as the μ^+ beam intensity was about 2.7 times higher than that of the μ^- beam. Second, the influence of shifted E_{miss} peak position as the E_{miss} distribution is not precisely centred at zero, but slightly shifted towards negative values, while it was observed certain SDME values depend on the position of the E_{miss} peak. Third, the dependence on the background angular distribution, where two methods in two different regions are compared to verify background angular distributions from LEPTO. Fourth, the uncertainty due to the background fraction determination, taken as 1% in case of ρ^0 and comparison of binned and unbinned maximum likelihoods methods in case of ω. Fifth, the sensitivity to the shapes of the kinematic distributions generated by HEPGEN, which is checked by repeating the extraction using reweighted MC events.

4. Results

The SDMEs extracted in the total kinematic region $5 < W < 17$ GeV/c^2, $1 < Q^2 < 10$ (GeV/c)^2, and $0.01 < p_T^2 < 0.5$ (GeV/c)^2 are presented in Fig. 2. These SDMEs are presented in five classes corresponding to different helicity transitions: A $\gamma_L^* \to V_L$ and $\gamma_T^* \to V_T$, B interference between the previous two, C $\gamma_T^* \to V_L$, D $\gamma_L^* \to V_T$, and E $\gamma_T^* \to V_{-T}$.

The kinematic dependences of the SDMEs on Q^2, p_T^2 and W are studied, as well as numerous observables and tests arising from SDMEs (mentioned in Sec. 1). More details can be found in [12]. In this report we focus on test of the SCHC hypothesis, where only the seven SDMEs of classes A and B are not restricted to vanish, while all SDMEs from classes C, D, and E should be equal to zero. Six of the SDMEs in classes A and B have to fulfil the following relations [6]:

$$r_{1-1}^1 = -\text{Im}\{r_{1-1}^2\}; \quad \text{Re}\{r_{10}^5\} = -\text{Im}\{r_{10}^6\}; \quad \text{Im}\{r_{10}^7\} = \text{Re}\{r_{10}^8\}. \tag{7}$$

The extracted SDMEs are consistent, within uncertainties, with these relations. However, for the transitions $\gamma_T^* \to V_L$ of class C the non-zero values of five unpolarised SDMEs indicate a clear SCHC violation as visible in Fig. 2.

Another useful test is to check contribution of the helicity-flip NPE amplitudes to the cross section of ρ^0, which can be quantified by the ratio τ_{ij} of the helicity-flip amplitudes T_{ij} to the square root of the sum of all amplitudes squared

$$\tau_{ij} = \frac{|T_{ij}|}{\sqrt{\mathcal{N}}}. \tag{8}$$

The ratios τ_{ij} can be expressed in terms of SDMEs as shown in Ref. [11]. Quantity τ_{01} describes the transition $\gamma_T^* \to V_L$, quantity τ_{10} describes the transition $\gamma_T^* \to V_L$, and quantity τ_{1-1} describes the transition $\gamma_{-T}^* \to V_T$. Results presented in Fig. 3 show significant deviation from zero values for τ_{01} and much smaller ones for τ_{10} and τ_{1-1}, which is consistent with the different degrees of SCHC violation seen for SDMEs in classes C, D and E.

The NPE-to-UPE asymmetry P of the transverse cross section for the transition $\gamma_T^* \to V_T$ is observable that is sensitive to the relative contributions of UPE and NPE amplitudes, defined in [13]. The kinematic dependences of the asymmetry P are shown in Fig. 4. The value of P for ρ^0 obtained in the total kinematic region is $0.887 \pm 0.016 \pm 0.029$, which indicates that NPE contribution dominates when averaged over the whole kinematic range of COMPASS. A small UPE contribution is observed only at small values of W and it becomes compatible with zero at larger W. ω shows very different behaviour, yielding P compatible with zero ($-0.007 \pm 0.076 \pm 0.125$), which indicates that the UPE
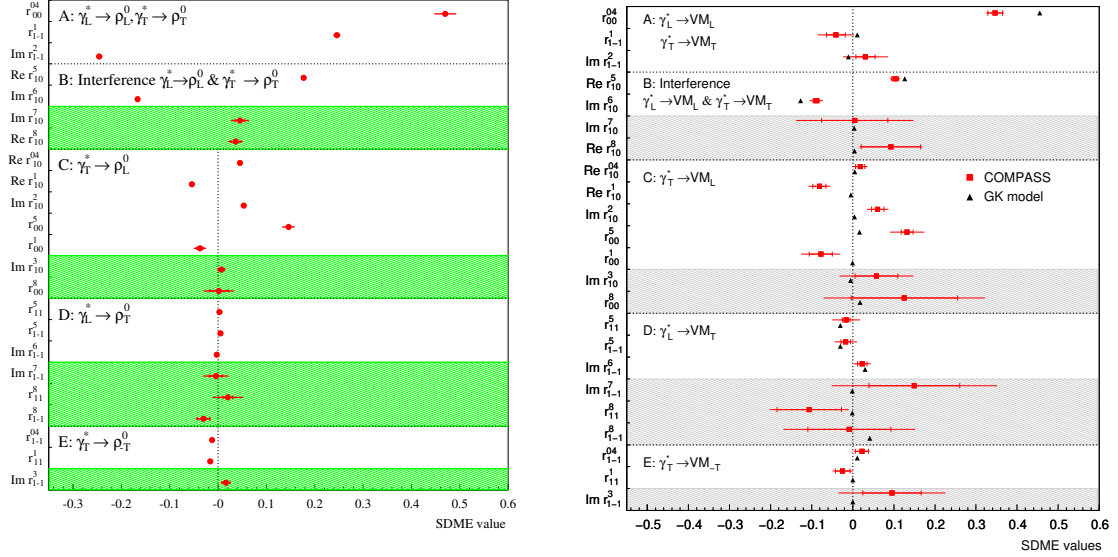
Fig. 2. The 23 SDMEs for exclusive ρ^0 (left) and ω (right) leptoproduction extracted in the total COMPASS kinematic region. Inner error bars represent statistical uncertainties and outer ones statistical and systematic uncertainties added in quadrature. Unpolarised (polarised) SDMEs are displayed in unshaded (shaded) areas. On the right, comparison of the measured SDMEs with calculations of the GPD model of Goloskokov and Kroll (GK Model) [13] is presented.
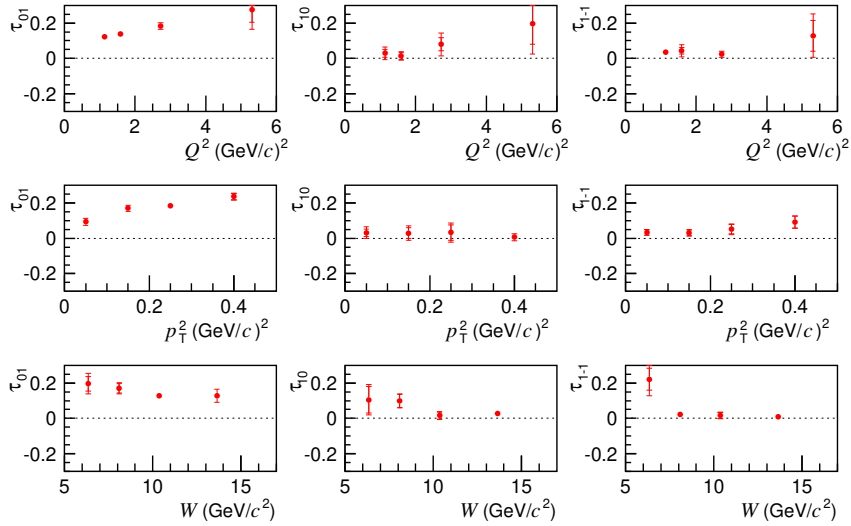

Fig. 3. Q^2, p_T^2 and W dependences of τ_{01}, τ_{10}, τ_{1-1} for the exclusive ρ^0 leptoproduction. Inner error bars represent statistical uncertainties and outer ones statistical and systematic uncertainties added in quadrature.

5

and NPE contributions averaged over the whole kinematic range are of similar size. The UPE contribution dominates at small values of W and decreases with increasing W. At large values of W the NPE contribution becomes dominant, while a non-negligible UPE contribution still remains.
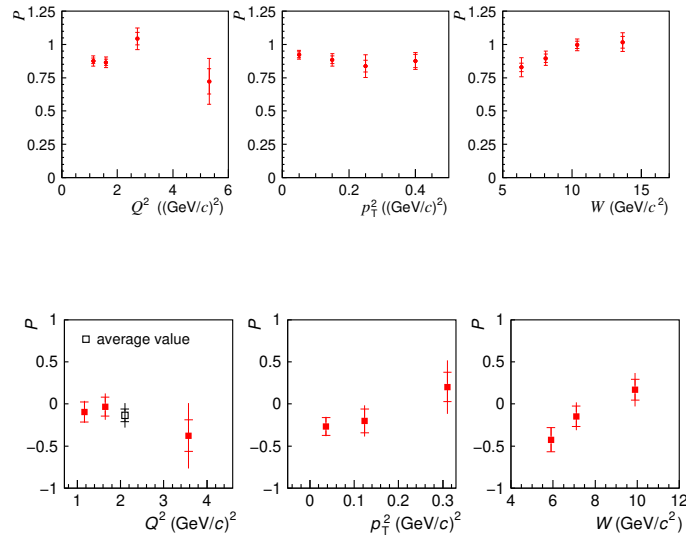

Fig. 4. Q^2, p_T^2 and W dependences of the NPE-to-UPE asymmetry of the transverse cross section for the transition $\gamma_T^* \to V_T$ for the exclusive ρ^0 (top) and ω (bottom) leptoproduction. Inner error bars represent statistical uncertainties and outer ones statistical and systematic uncertainties added in quadrature.

5.   Summary

Measurement of 23 SDMEs using ρ^0 and ω Mesons at COMPASS was presented. SDMEs describing the transitions $\gamma_T^* \to V_L$ indicate a clear SCHC violation. Consistent SCHC violation is observed in the τ_{01} ratio of the helicity-flip NPE amplitudes for the ρ^0 meson. These SDMEs are expected to be sensitive to the chiral-odd GPDs H_T and $\bar{E}_T$, which are coupled to the higher-twist wave function of the meson. Specific observables were used to estimate the relative contributions of UPE and NPE amplitudes.

References

[1] A.C. Irwing and R.P. Worden, Phys. Rep. **C34**, 117 (1977).
[2] D. Müller et al., Fortschr. Phys. **42**, 101 (1994).
[3] X. Ji, Phys. Rev. D **55**, 7114 (1997).
[4] A.V. Radyushkin, Phys. Rev. D **56**, 5524 (1997).
[5] J.C. Collins, L. Frankfurt, M. Strikman, Phys. Rev. D **56**, 2982 (1997).
[6] K. Schilling and G. Wolf, Nucl. Phys. B **61**, 381(1973).
[7] M. Diehl, JHEP **0709**, 064 (2007).
[8] P. Abbon et al. (COMPASS Collaboration), Nucl. Instrum. Meth. A **557**, 455 (2007).
[9] P. Abbon et al. (COMPASS Collaboration), Nucl. Instrum. Meth. A **779**, 69 (2015).
[10] C. Adolph et al. (COMPASS Collaboration), Phys. Lett. B **731**, 19 (2014).
[11] A. Airapetian et al. (HERMES Collaboration), Eur. Phys. J. C **62**, 659 (2009).
[12] G.D. Alexeev et al. (COMPASS Collaboration), Eur. Phys. J. C **81**, 126 (2021).
[13] S.V. Goloskokov, P. Kroll, Eur. Phys. J. A **50**, 146 (2014).